GeoScienceWorld
Lithosphere
Volume 2022, Article ID 9120724, 18 pages
https://doi.org/10.2113/2022/9120724

Lithosphere

Research Article

Internal Architectural Patterns of Bar Fingers Within Digitate Shallow-Water Delta: Insights from the Shallow Core, GPR and Delft3D Simulation Data of the Ganjiang Delta, China

Zhenhua Xu,[1,2] Shenghe Wu,[1,2] Quanlin Wang,[3] Pan Zhang,[4] Meng Deng,[3] Wenjie Feng,[5] Jiajia Zhang,[1,2] and Changmin Zhang[5]

[1]*State Key Laboratory of Petroleum Resources and Prospecting, China University of Petroleum-Beijing, Beijing, 102249, China*
[2]*College of Geosciences, China University of Petroleum-Beijing, Beijing, 102249, China*
[3]*Bohai Petroleum Research Institute, CNOOC Tianjin Branch, Tianjin, 300459, China*
[4]*Oil Production Plant 11, Changqing Oilfield Branch of PetroChina, Qingyang, 745000, China*
[5]*College of Geosciences, Yangtze University, Wuhan, 430100, China*

Correspondence should be addressed to Changmin Zhang; zcm@yangtzeu.edu.cn

Received 9 June 2022; Accepted 29 June 2023; Published 31 July 2023

Academic Editor: Feng Cheng

Digitate shallow-water deltas are commonly found in modern lakes and bays, as well as within cratonic petroliferous basins. They develop one or multiple sinuous finger-like sands (i.e., bar fingers), including high-R_{SI} (sinuosity ratio of distributary channel and bar finger ≥1) and low-R_{SI} (R_{SI} < 1) types. Bar fingers consist of four types of subenvironments, that is, distributary channels, point bars, mouth bars, and levees. However, the internal architecture within the above subenvironments is still unclear. This paper documents the internal architecture of a digitate delta based on the integration of shallow-core and ground-penetrating radar data from the Ganjiang Delta, China, coupled with Delft3D simulations. Our results show that multiple convex-up muddy-silty accretion beds are developed in mouth bars, which top lap the side of the distributary channels or point bars and down lap the bottom of the mouth bar. The accretion beds have low dip angles (<2°), which is slightly higher for the upper accretion beds. Point bars, unique to the high-R_{SI} bar finger, develop multiple inclined silty drapes, which top lap the top of the point bar. The cohesive levee and backwater effect impede the migration of the distributary channel, resulting in silty drapes with high-dip angles (can be >10°) compared with those in the supplying river. This dip angle exhibits a negative relationship with downstream distance and a positive exponential relationship with lateral migration distance. Silty drapes become dense along the migration direction of the distributary channel. The levee develops multiple horizontal muddy accretion beds. The high-R_{SI} bar finger develops a large number (>3) of accretion beds in mouth bars with high dip angles, and a large number of accretion beds in thick levees, compared with the low-R_{SI} bar finger. The results of this paper provide insights into the prediction and development of cratonic digitate shallow-water delta reservoirs.

1. Introduction

River-dominated deltas are among the most important landforms on earth because they host extensive wetlands, major ports, and cities, and their ancient deposits host proliferous hydrocarbon reserves. Thus, much work has gone into understanding their morphology, architecture, and formative processes [1–4].

Lobate and digitate deltas are two end-member morphological types of river-dominated deltas [5–9]. Lobate deltas develop coeval terminal distributary channels and sheet sands, attributed to frequent channel bifurcations, and distributary channel incision into the sides of mouth bars as found in such systems as the Wax Lake Delta and Mossy Delta [7–10]. In contrast, digitate deltas develop one or multiple finger-like sands (termed bar fingers, see

Reference 11) that consist of distributary channels, mouth bars, and levees, and individual bar fingers are separated by interdistributary bays, such as within the Mississippi Delta and Birch River Delta [11–19]. Sediment properties provide the first-order control on the morphology of river-dominated deltas: fine-grained, high-cohesive deltas have a digitate shape with bar fingers, whereas coarse-grained, low-cohesive deltas are lobate shape with sheet sands [9, 10, 20, 21].

Water depth also controls deltaic morphology [13, 21, 22]. Shallow-water deltas form in a few meters of water, and the water depths at the distributary outlet are shallower than that in the distributary channel. In contrast, deep-water deltas form in tens to hundreds of meters of water, and the water depths at the distributary outlet are deeper than distributary channel depths.

This paper examines the bar fingers of a digitate shallow-water delta, which commonly develop in modern bays and lakes (e.g., Guadalupe Delta, San Antonio Bay, USA; Wulan Delta, Java Sea, Indonesia; Peace-Athabasca Delta, Lake Claire, Canada; Ganjiang Delta, Poyang Lake, China), as well as in petroliferous cratonic basins (e.g., Triassic Yanchang Formation, Ordos Basin, China; Neogene Minghuazhen Formation, Bohai Bay Basin, China). Scholars have studied the architecture and formative processes of bar fingers of digitate shallow-water deltas and pointed out that bar fingers are sinuous and consist of mouth bar, distributary channel, levee deposits, and, sometimes, point bar deposits [16, 23, 24]. Bar fingers have two types of depositional architectures, determined by the sinuosity ratio of distributary channel and bar finger (R_{SI}): high-R_{SI} bar fingers ($R_{SI} \geq 1$) develop high-sinuosity distributary channels (sinuosity index ≥ 1.2) with point bars at inner banks of the distributary channel; while low-R_{SI} bar fingers ($R_{SI} < 1$) develop low-sinuosity distributary channel (sinuosity index < 1.2) without point bar deposits [24]. However, the internal architecture and formative mechanism of the facies (including mouth bars, distributary channels, point bars, and levees) within low-R_{SI} and high-R_{SI} bar fingers remain unclear.

Shallow cores and ground penetrating radar (GPR) profiles are commonly used to explore the architecture of modern deposits. Fisk [11] and Donaldson [16] adopted shallow cores to investigate the architecture of bar fingers within the Mississippi River Delta and the Guadalupe Delta, respectively [11, 16]. The intercore variability makes it difficult to predict the internal architecture of a single facies. GPR profiles allow the examination of the internal architecture of modern deposits, such as point bars in rivers [25, 26] and mouth bars in deltas [27, 28], at the decimeter scale. In addition, Delft3D software is widely used to simulate digitate and lobate shallow-water deltas, which can simulate the sedimentary processes and architecture in the natural system [9, 10, 24].

Based on fieldwork (shallow cores and GPR profiles) and Delft3D simulations of the Ganjiang Delta within Poyang Lake, China, this study aims to examine the internal architecture of low-R_{SI} and high-R_{SI} bar fingers and investigate the formative mechanisms. Finally, we utilized these internal architectural patterns to give insights into the development of bar finger reservoirs in two cratonic petroliferous basins in China: Ordos Basin and Bohai Bay Basin.

2. The Study Area

Poyang Lake is the largest freshwater lake in China. It is located in northern Jiangxi Province. Poyang Lake is 110 km long and 50–70 km wide and covers an area of 4125 km^2 [28, 29]. Its bottom slope is <0.05°, its average water depth is 8.4 m, and it experiences relatively little wave energy [30]. The Ganjiang, Fuhe, Raohe, Xinjiang, and Xiushui Rivers flow into Poyang Lake, resulting in the formation of numerous deltas [31, 32]. The Ganjiang River is the largest river among them and bifurcates at Nanchang into four distributary channels, which flow into the western side of the Poyang Lake and form the Ganjiang Delta near the Nanchang City [31] (Figure 1(a) and (b)). Ganjiang Delta, the largest delta in Poyang Lake, is a typical shallow-water delta. The water depth of its distributary channels is 1.0–1.3 times the lake's water depth [24]. The Ganjiang Delta can be divided into an upper delta plain, a lower delta plain–delta front, and a prodelta. The Ganjiang Delta contains multiple digitate delta lobes with bar fingers in the lower delta plain-delta front (Figure 1(c)). We conducted a detailed study of two bar fingers (BSD5 and BSD6 in Figure 1(c)) to examine the internal architecture of the bar fingers of digitate shallow-water deltas. BSD5 and BSD6 are high-R_{SI} and low-R_{SI} types, respectively [24].

3. Data and Methods

3.1 Field Work. Shallow cores and GPR data were acquired on BSD5 and BSD6 in the Ganjiang Delta to document the sedimentology and architecture of the bar fingers.

3.1.1 Shallow Core Data Acquisition. Shallow cores, including shallow drill cores and exploratory pits, were acquired using a portable vibrating drilling machine (Figure 2(a)) and shovel, respectively (Figure 2(b)). Combined with particle size analysis, we documented the sedimentary characteristics of ninety-nine shallow cores (sixty-five in BSD5 and thirty-four in BSD6) at the centimeter scale. These data were used to generate four and five cross-sections in the BSD5 and BSD6, respectively (Figure 3). The distances between adjacent shallow cores in the cross-sections were mostly <50 m.

3.1.2 GPR Acquisition. GPR profiles were acquired with an RIS GPR from IDS Company, Italy, with a 200 MHz antenna (Figure 2(c)). The RIS GPR equipment was imaged to depths of approximately 3 m, with a vertical resolution of 5–10 cm. After GPR data acquisition, five processing steps were conducted including zero-time adjustment, background noise removal, vertical bandpass filtering, lateral event smoothing, and vertical gain. The zero-time adjustment was used to remove the ground wave. Background noise removal was used to remove most of the noise in the GPR profile. The vertical bandpass filtering aimed to reduce the vertical artificial reflected-wave discontinuities

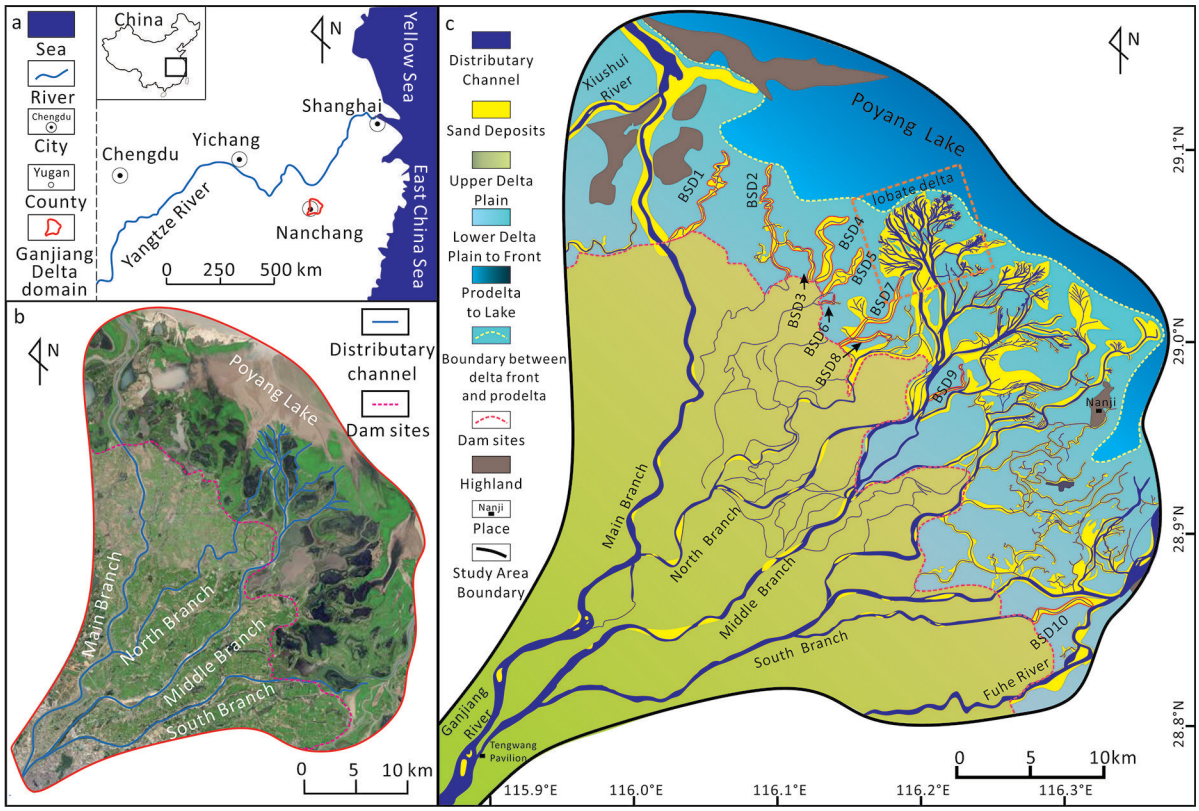

Figure 1: (a) Location of the modern Ganjiang Delta. (b) Satellite image of the Ganjiang Delta and its four distributary channels. (c) Major environments and deposits of the Ganjiang Delta (modified from reference 24). Also, shown are ten bar fingers (BSD1–BSD10) and one lobate bar developed in the lower delta plain-delta front.

caused by rough ground, and lateral event smoothing reduced lateral reflected-wave discontinuities caused by the antenna's unsteady movement speed. The vertical gain was used to reduce the impacts of vertical energy decay.

The GPR data were converted into the depth domain based on the average velocity (approximately 0.1 m/ns [25]). The SSOKKIA bubble-level equipment was used to measure the elevation profiles of the bar fingers (Figure 2(d)) to correct the GPR profiles for topography. We collected two GPR profiles in the BSD5 and six GPR profiles in the BSD6, which partly coincided with the location of shallow cores (Figure 3).

3.2 Delft3D Simulation. Delft3D is an effective software for simulating the depositional process of the digitate shallow-water delta with bar fingers [9, 10, 24].

3.2.1 Delft3D Model Description. Delft3D is a process-based numerical model developed by Deltares to simulate fluid flow and sediment transport [33, 34]. In the Delft3D model, the influences of evaporation, precipitation, the Coriolis force, wind, and waves are neglected. Flow is assumed as an incompressible fluid and is computed by the depth-averaged, Reynolds-averaged Navier-Stokes equations [10].

The sediments are divided into cohesive muds and noncohesive sands [9]. The cohesive muds are defined as grain sizes <64 μm and are considered suspended loads. In contrast, the noncohesive sands with grain sizes of ≥64 μm could be suspended or bed loads. Formulas from van Rijn [35] were used to calculate both suspended and bedload transport [35].

3.2.2 Delft3D Model Setup. The domain and simulated parameters of the Delft3D model were set based on satellite and field data from the modern Ganjiang Delta. The model domain was 10 × 8 km with 40 × 40 m grid cells (Figure 4(a)). The catchment basin dominated the model area, with an initial basinal bed slope of 3.75×10^{-4}. The initial supplying river was located in the south of the model, with a 240 m width and 2.5 m depth. Seasonal variations of hydrology were not considered. The water discharge and sediment concentration were set at ~1200 m^3/s and 0.1 kg/m^3, respectively, based on hydrologic data from the Ganjiang River [30, 36]. The sediments were a mixture of six components, whose D50 are 300, 150, 80, 32, 13, and 7.5 μm, and their contents are 5%, 5%, 20%, 40%, 20%, and 10%, respectively. The sediment cohesion was quantified by critical shear stress for the erosion of the cohesive sediment, which was ~0.2 N/m^2 [37]. Weak wave processes in the Ganjiang Delta were ignored [37].

The simulation ran for 320 simulated hours. The time step was 0.1 minute. The morphological scale factor was 175 to allow an increased rate of morphological changes [9]. If considering 10 days per year of bankfull conditions [10],

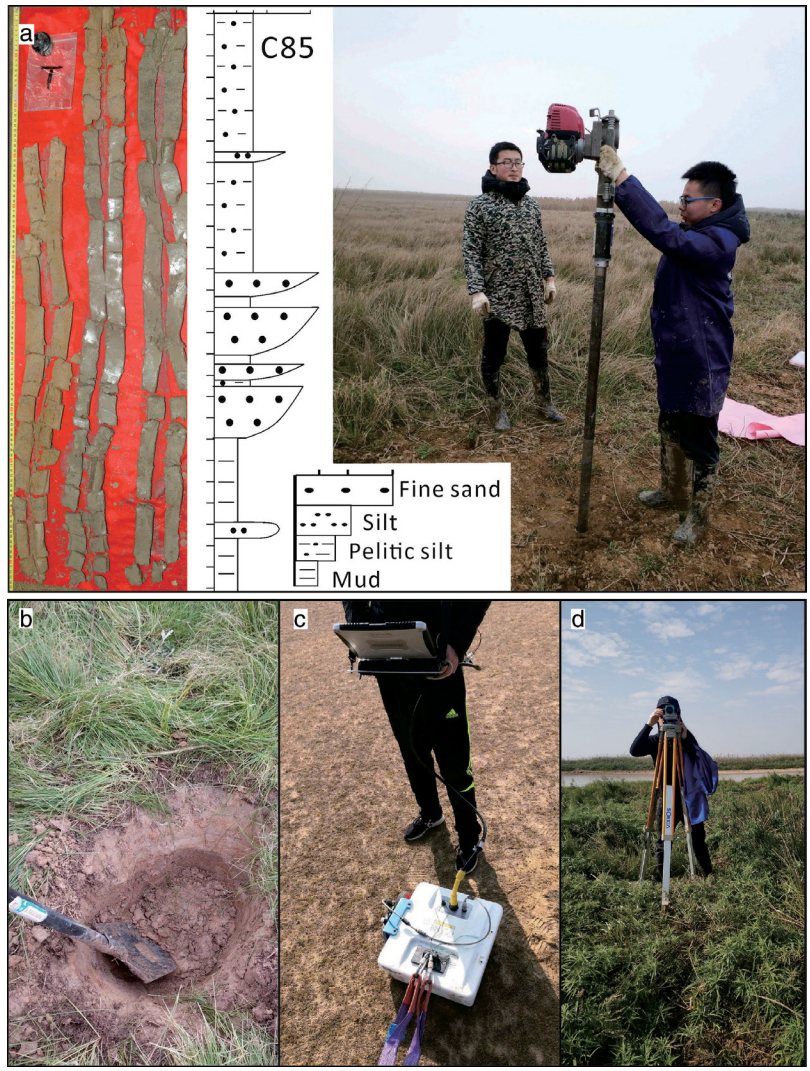

Figure 2: Fieldwork, equipment, and data from the Ganjiang Delta. (a) Collection, photograph, and description of a typical shallow core (No. c85); (b) photograph of an exploration pit; (c) RIS GPR equipment with a 200 MHz antenna; and (d) SSOKKIA bubble-level equipment.

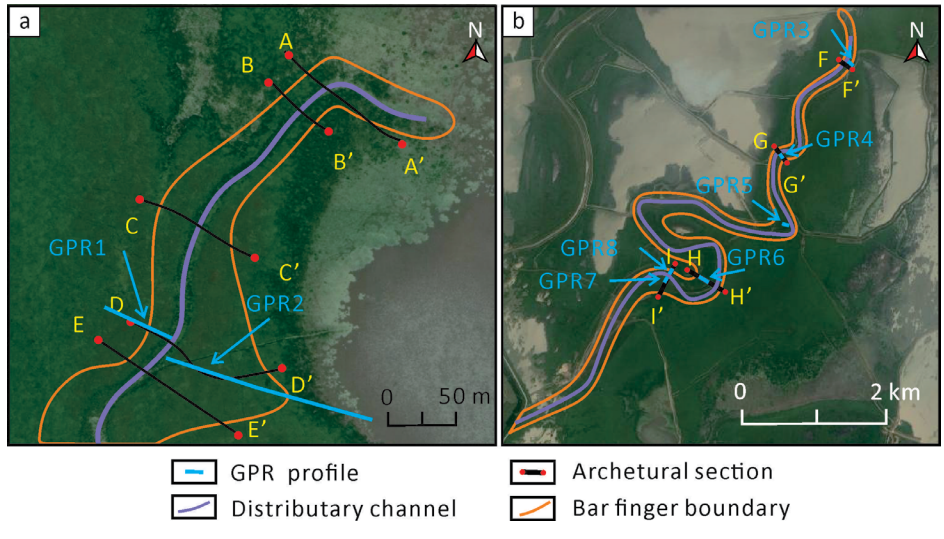

Figure 3: Cross-sections and GPR profiles in BSD5 (a) and BSD6 (b).

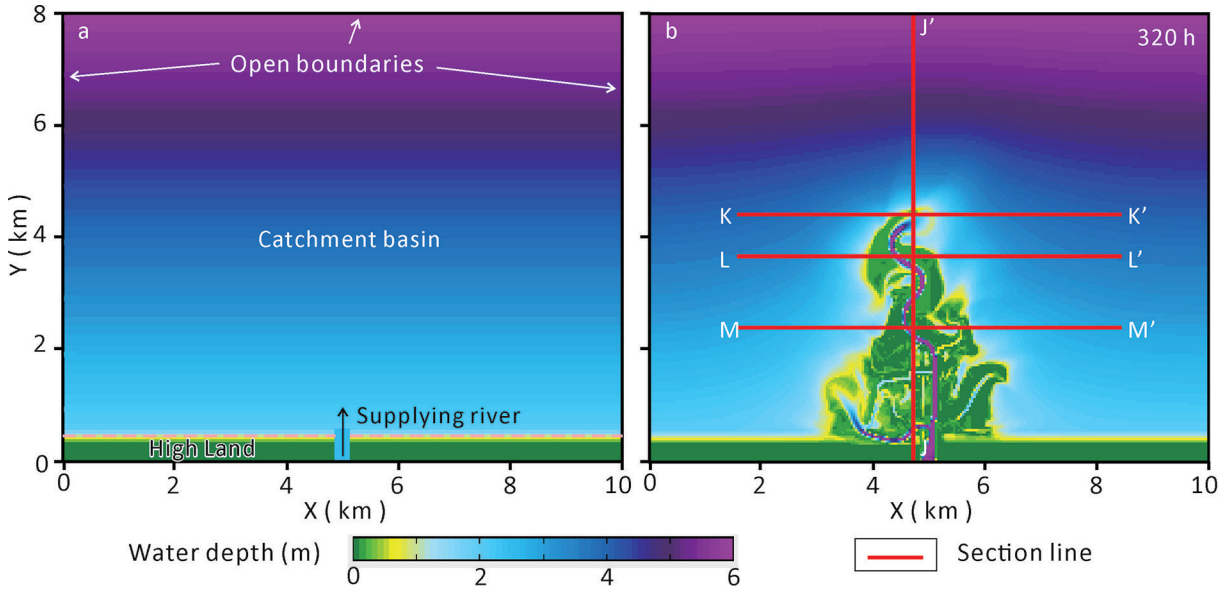

Figure 4: Delft3d model domain (a) and simulation results (b).

the simulation represents a period of ~233 years in nature. These parameters allowed for the development of a digitate shallow-water delta with bar fingers (Figure 4(b)).

4. Results

4.1 Modern Bar Finger: Architecture Units and GPR Response. The digitate delta is composed of one or multiple bar fingers, which consist of mouth bar, distributary channel, levee, and point bar deposits, separated by bay/lake deposits (Figure 5 [24]). According to the architectural hierarchy scheme of Wu et al. [38], a six-level architectural unit corresponds to single-stage sedimentary facies, a seven-level architectural unit corresponds to the main genetic unit during the largest autogenic cycle, an eight-level architectural unit corresponds to a macroform, and a nine-level architectural unit corresponds to accretion within a macroform [38]. A single-stage digitate delta is a six-level architectural unit, and a bar finger and bay/lake are seven-level architectural units. Within bar fingers, the mouth bar, distributary channel, levee, and point bar comprise all eight-level architectural units, and their accretion sand bodies and beds constitute nine-level architectural units. Here, we focus on the eight-level and nine-level architectural units within the bar finger. Distributary channels within BSD5 and BSD6 are abandoned and are filled by standing water and muddy deposits. Their architectures are not the focus of this paper.

We chose a point bar (Laozhoutou point bar) in the Ganjiang Delta plain to analyze GPR responses to modern deposits in the Ganjiang Delta (Figure 6(a)). Trench data show that the Laozhoutou point bar consists of multiple lateral accretion sand bodies and dark silty drapes (Figure 6(b)). The thickness of lateral accretion sand bodies is about 10 cm. The largest dip angle between the silty drapes and the horizontal plane is about 3°. Assuming the central line of silty drapes is resolvable (black peak in the GPR profile), the GPR profile recorded the vertical thickness and dip angle of the lateral accretion sand bodies (Figure 6(d)). We hypothesize that the peak in the GPR profile represents the fine-grained accretion beds, and the GPR responses within the bar finger can be integrated with shallow cores (Figure 5).

The mouth bars (Figure 5(a)) consist of gray coarsening-upward, medium, and fine sands, with tabular cross-stratification and planar lamination. Its deposits have flat bases and convex-up tops in cross section. In GPR profiles, the mouth bar is marked by a wedge reflection with a horizontal base and arched top. Within the mouth bar deposits, multiple muddy-silty accretion beds separate coarsening-upward accretion sand bodies. The accretion beds are marked by convex-up reflections almost parallel to the top of the mouth bar in the GPR profile (Figure 6(a)).

The point bars (Figure 5(b)) consist of brown or gray, fining-upward, medium-fine sands, with wedge-shaped to trough cross-stratification. They have scoured bases and horizontal tops in the flow direction. In the GPR profiles, the point bar has an incised base and horizontal top. The point bar deposits contain multiple silty drapes that separate fining-upward lateral accretion sand bodies. The silty drapes are marked by inclined reflections.

The levees (Figure 5(c)) consist of brown silty mud and some silty sands, which display a weakly developed fining-upward sequence and plant roots. They contain horizontal accretion beds and sand bodies. In the GRP profiles, levee and inner accretions are marked by parallel reflections.

The bay/lake (Figure 5(d)) deposits consist of dark mud with plant fragments. Its sediments are highly cohesive and commonly covered by standing lake water. In GPR profiles, their deposits are marked by discontinuous undulate reflections.

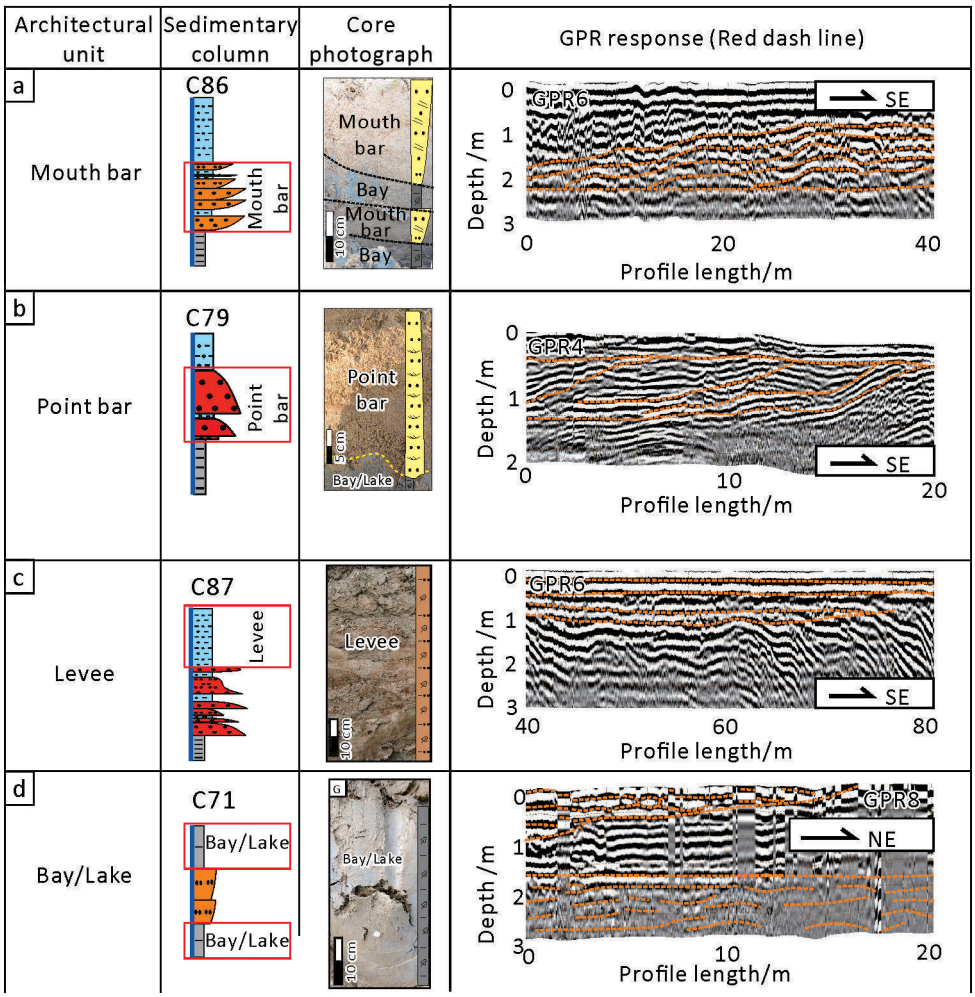

FIGURE 5: Core descriptions, photographs, and GPR profiles from eight-level architectural units, including mouth bar (a), point bar (b), levee (c), and bay/lake (d).

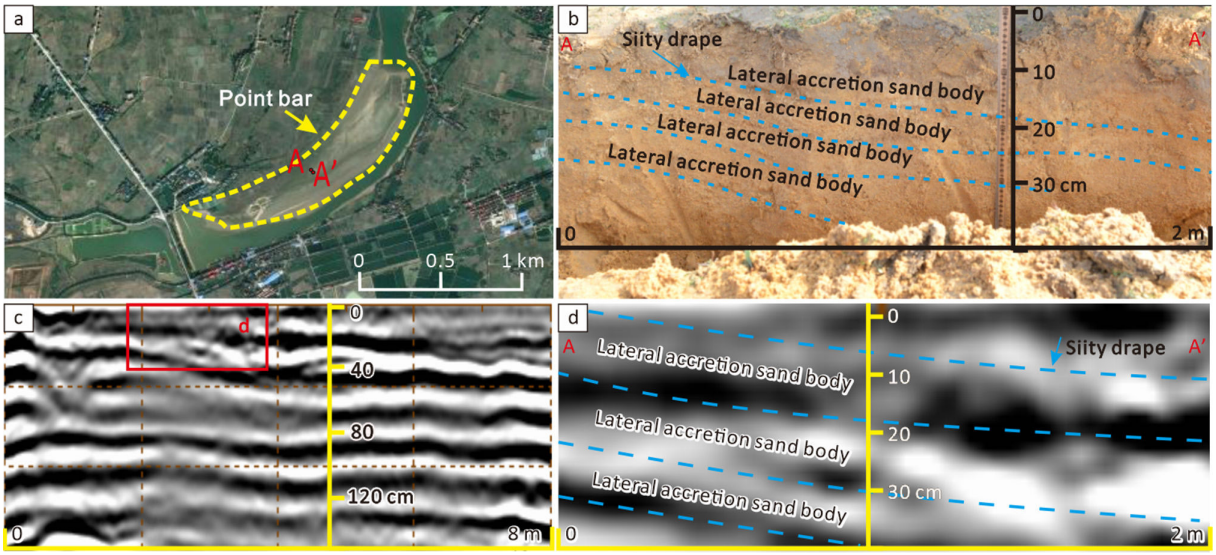

FIGURE 6: A point bar (Laozhoutou point bar) in the Ganjiang Delta plain. (a) Satellite image. (b) Lateral accretion sand bodies and silty drapes in a trench. (c) GPR profile. (d) Inset of GPR profile in subplot c, corresponding to the trench.

4.2 Modern Bar Finger: Architectural Unit Distribution. For low-R_{SI} BSD6 and high-R_{SI} BSD5, Xu et al. [24] documented the distribution of the eight-level architectural units with shallow cores. Here, we redescribed the distribution of eight-level architectural units and revealed the distribution of the nine-level architectural units by integrating shallow core and GPR data (Figures 7 and 8).

4.2.1 Architectural Unit Distribution of Low-R_{SI} BSD6. GPR profiles show the architectural unit distribution of the inner bank and outer bank of the distributary channels, respectively (Figure 3). The mouth bars are dominated by sandy deposits within BSD6, which have a flat base and a convex top (Figure 7). Mouth bar deposits are thicker and wider at the outer bank (GPR2) compared with the inner bank (GPR1; thickness: 0.45 vs. 0.15 m; width: 105 vs. 28 m), and the thickest section (near the core C50) is also located on the outer bank. The thicker mouth bar deposits induce higher topography at the outer bank, compared with the inner bank. The levee is accreted at the top of the mouth bar, which is 1/5~3/4 times thinner and slightly wider than the mouth bar. It is thinnest where the mouth bar is thickest (Figure 7). In contrast, there are no point bar reflections (incised base and inclined reflection) in GRP profiles. It suggests point bars are not developed in the low-sinuosity BSD6, as proposed by Xu et al. [24].

Within mouth bars, we observed multiple accretion beds (nine-level architectural units), which exhibit similar convex-up shapes as the top of the mouth bar (Figure 7). They are the highest at the location of the thickest mouth bar and intersect the bottom of the mouth bar. The dip angle of the accretion bed is less than 1° (0.15°–0.7°), and it is higher at the outer bank of the distributary channel (GPR2), compared with the inner bank (GPR1; 0.6° vs. 0.2° in average). The coarsening-upward accretion sand bodies are interbedded with muddy-silty accretion beds (columns in Figure 7). The accretion sand bodies are thickest and coarsest near the central mouth bar (C50 in Figure 7).

Within the mouth bars, there are two muddy-silty accretion beds, resulting in three convex-up accretion sand bodies (sections C-C'–E-E' in Figure 8), except for the thin terminal mouth bar, which developed only one accretion sand body (sections A-A' and B-B' in Figure 8). In the proximal mouth bar, the accretion sand bodies are coarse-grained, and muddy-silty accretion beds are thin (<5 cm) and discontinuous with low dip angles (sections D-D' and E-E' in Figure 8). In the middle sections of the bar finger, the accretion sand bodies are also relatively coarse-grained, and muddy-silty accretion beds are thicker (0.2, 10 cm) and more continuous with high dip angles (section C-C' in Figure 8). In the terminal bar finger, only one accretion sand body is developed, which is fine-grained and thin (Sections A-A' and B-B' in Figure 8).

4.2.2 Architectural Unit Distribution of High-R_{SI} BSD5. GPR profiles show the architectural unit distribution of high-R_{SI} BSD5 at both banks of the distributary channels and different downstream locations (Figure 3). Mouth bars and point bars are both dominated by sandy deposits within BSD5 (Figure 9). The mouth bar has a flat base and a convex top, whereas the point bar has a convex base and a relatively flat top. The point bar incises the part of the mouth bar, resulting in an erosional contact (GPR4–GPR6 in Figure 9). It is about 120% thicker than the mouth bar and is 50%–75% thinner near the mouth bar bank compared with that near the distributary channel. The mouth bar is thickest near the distributary channel and point bar (GPR3 and GPR4 in Figure 9) but becomes thinner and gradually pinches out at the sides of the mouth bar (GPR3 and GPR8 in Figure 9). A thick levee (0.5, 2.0 m) overlays the mouth bar and point bar deposits and is thinnest near the central mouth bar or on the point bar (C79 and C94 in Figure 9) and also thins toward the margins of the Bird-foot deltas (BSDs), away from the channels (GPR8 in Figure 9). BSD5 has a high elevation and relatively flat topography because of the accretion of the levee.

Within the mouth bar of BSD5, we recognized 2–5 accretion beds (nine-level architectural units; Figure 9; Figure 7). The convex-up accretion beds top lap the side of the point bar or distributary channel and down lap the bottom of the mouth bar. The dip angle of the accretion beds is 0.8°–1.6° and is similar to that in GPR profiles (Figure 10(a)). It slightly increases basinward (from GPR7 to GPR3). Vertically, the upper accretion bed has a higher dip angle than the lower accretion bed (e.g., 1.5° vs. 1.2° in GPR4). The coarsening-upward accretion sand bodies are interbedded with the muddy-silty accretion beds. Within the point bar, we observed multiple inclined accretion beds (i.e., silty drapes), which top lap the top of the point bar (such as GPR7 in Figure 9). The dip angle of the silty drapes ranges from 4° to 15° and is a function of downstream distance and migration distance (Figure 10(c) and (d)). The dip angle of silty drapes decreases basinward (from GPR7 to GPR4, the average value from 9.8° to 5.3°, illustrated in Figure 10(c)). In addition, the dip angle exponentially increases with lateral migration distance (Figure 10(d)). The fining-upward accretion sand bodies are interbedded with silty drapes. The lateral spacing between adjacent silty drapes is 1/2–1/3 times smaller on the distributary channel side compared with the interdistributary bay side (GPR7 in Figure 9). Within the levee, we also recognized multiple horizontal accretion beds that are parallel to the top of the mouth bar (Figure 9).

Based on our data, we expand the model of BSD5 of Xu et al. [24] (Figure 11). We modified the architectural boundary of the point bar and described the accretion sand bodies and beds in the mouth bars, point bars, and levees. 3–5 convex-up accretion sand bodies in the mouth bar, vertically separated by 2–4 accretion beds, which thin from the center to the margin of the mouth bar (Figure 11). Dozens of silty drapes in the point bar are developed, which are steeper and denser on the convex margin of the point bar than on the concave margin (C87 vs. C88 in Figure 11). The middle-upper lateral accretion sand bodies are separated by silty drapes, while the lower lateral accretion sand bodies are connected. In the proximal bar finger (sections H-H' and I-I' in Figure 11), mouth bars and point bars contain coarse-grained and thick accretion sand bodies. The mouth bars develop 2–4 accretion beds, and the

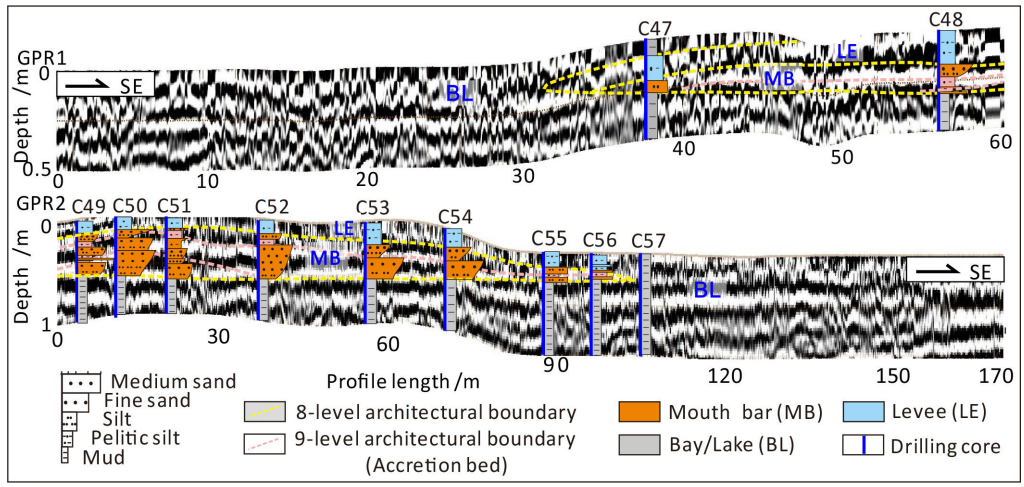

FIGURE 7: GPR cross profiles (GPR1 and GPR2) and the distribution of the eight- and nine-level architectural units within BSD6. Locations of the GPR profiles are shown in Figure 3.

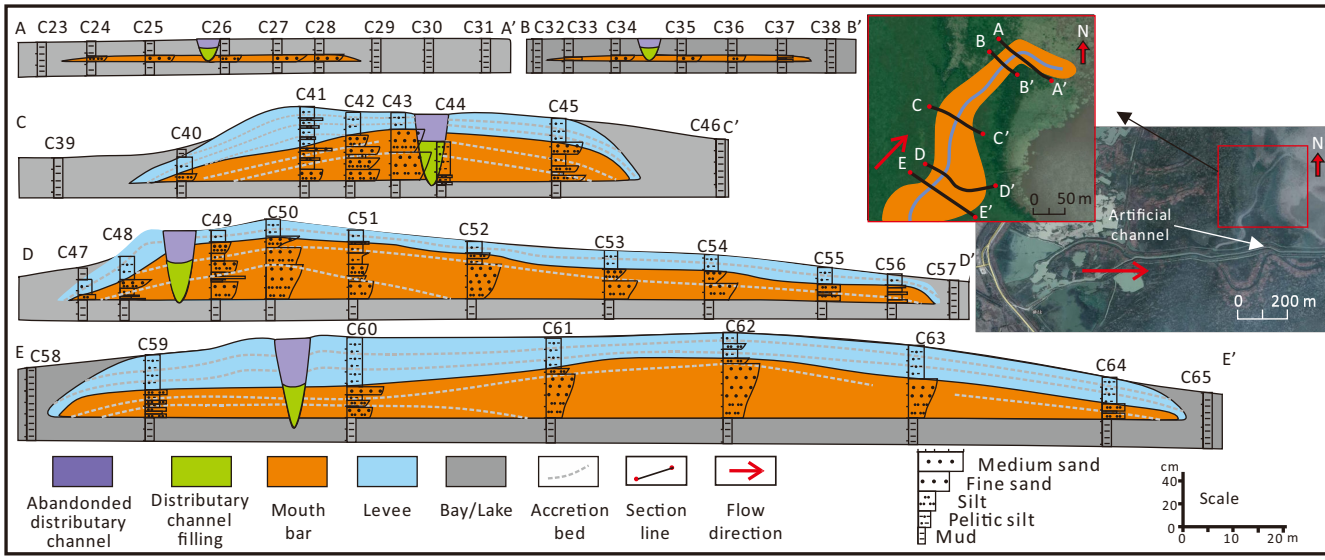

FIGURE 8: Distribution of architectural units within BSD6. The locations of the five cross-sections are indicated in the inset in the right corner as well as in Figure 3.

point bars develop 13–18 silty drapes with high dig angles (~9°). In the middle sections of the bar finger (section G-G' in Figure 11), the accretion sand bodies in the mouth bars and point bars are also relatively coarse-grained and thick. The mouth bars contain ~2 accretion beds, and the point bars contain ~3 silty drapes with low dig angles (~5°). In the terminal bar finger (section F-F' in Figure 11), the point bar is commonly not developed, and the accretion sand bodies in the mouth bars are fine-grained and thin, which are separated by ~2 accretion beds.

4.3 Simulated Bar Finger: Architectural Characteristics and Formative Processes. A digitate shallow-water delta with five low-R_{SI} bar fingers (sinuous indexes are all <1.2) is simulated by Delft3D (Figure 5(b)), which illustrates the architectural characteristics and formative processes of low-R_{SI} bar fingers. This paper takes the central bar finger as an example to describe the architectural characteristics and formative processes.

4.3.1 Architectural Characteristics. The longitudinal section illustrates the topset, foreset, and bottomset of the bar finger based on changes in slope and grain size (Figure 12(a) and (b)), which represent levee, mouth bar, and prodelta-lake deposits. The mouth bars contain multiple accretion sand bodies with coarse grain sizes (50, 100 μm) and high dip angles (0.1°–0.3°), whereas the levees develop multiple horizontal accretion sand bodies with fine grain sizes (<50 μm). The dip angles of accretion beds in the mouth bars decrease downstream from 0.3° to 0.1° (Figure 12(a)) and accretion beds fine downstream (Figure 12(b)).

The cross sections show that the central bar finger is thick and coarse-grained and becomes thin and fine-grained from the central to marginal bar finger (Figure

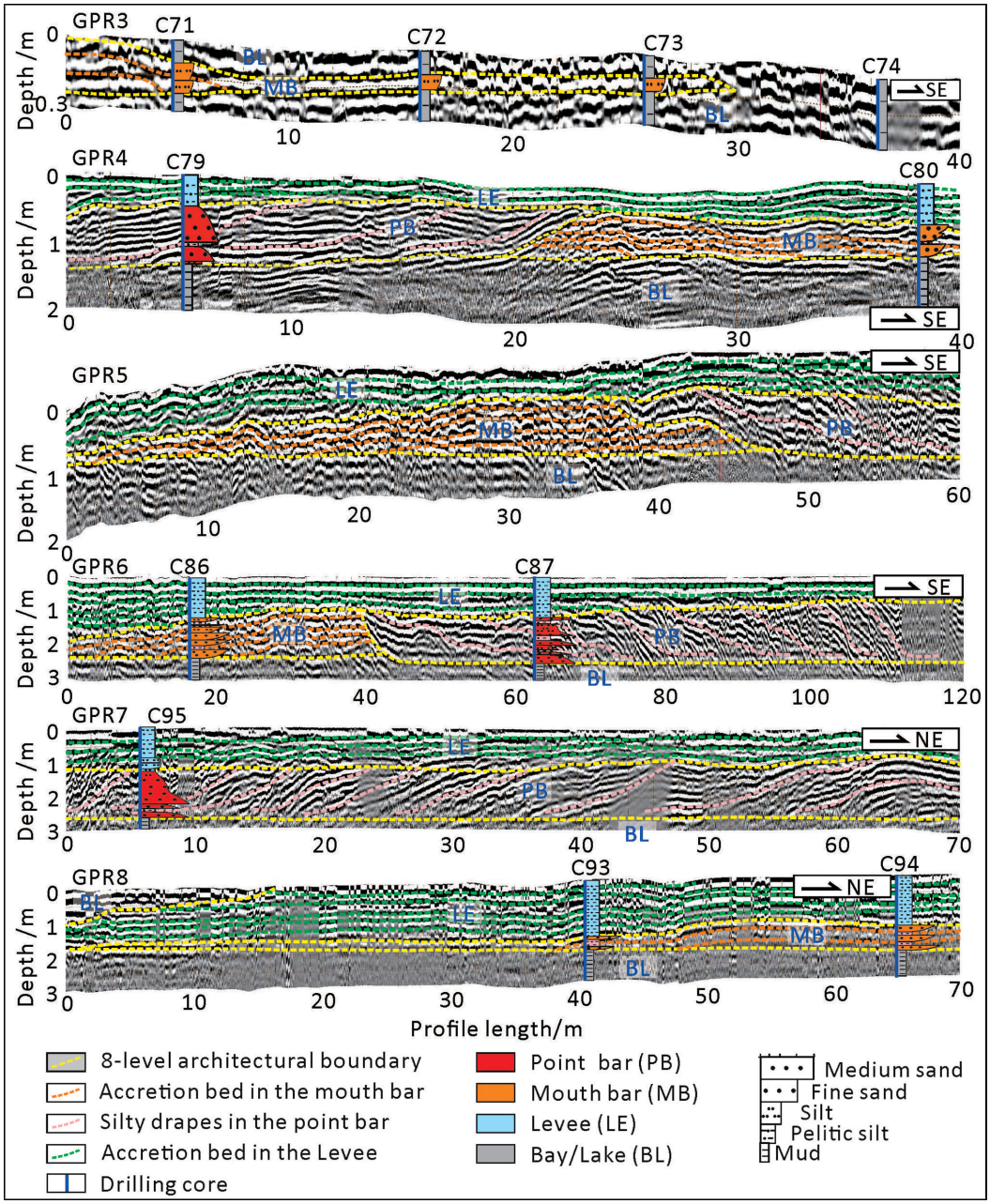

Figure 9: GPR profiles (GPR3–GPR8) and the distribution of eight- and nine-level architectural units of BSD5. The locations of the six GPR profiles are shown in Figure 3.

12(c)–12(h)). The accretion beds in the mouth bars are convex-up shaped, and their dip angle (from 0.6° to 0.3°) and grain size (from 80 to 40 μm) decrease downward (Figure 12(c)–12(h)).

4.3.2 Formative Processes. In the simulation, the flow velocity gradually increased during 128–176 hours (black circle, Figure 13(a)–13(c)). As a result, a narrow mouth bar was formed at 144 hours, and it gradually thickened and widened (Figure 14(b) and 14(c)), leading to an upward-coarsening sequence and convex-up accretion beds during 144–176 hours (Figure 12(g) and 12(h)). During 176–224 hours, the distributary channel extended beyond the black circle, and flow velocity decreased (Figure 12(d)–12(f)). As a result, fine-grained and suspended-load sediments were accreted on the top of the mouth bar (Figure 13(c)–13(f)) and formed thin and fine levees within horizontal accretion beds (Figure 12(g) and 12(h)).

5. Discussion

5.1 Architectural Patterns Within Bar Fingers of Shallow-Water Delta. Previous work has focused on bar fingers within deep-water deltas (e.g., Mississippi Delta) and their architecture [8, 13, 39, 40]. However, the architecture of the bar fingers within shallow-water deltas has received less

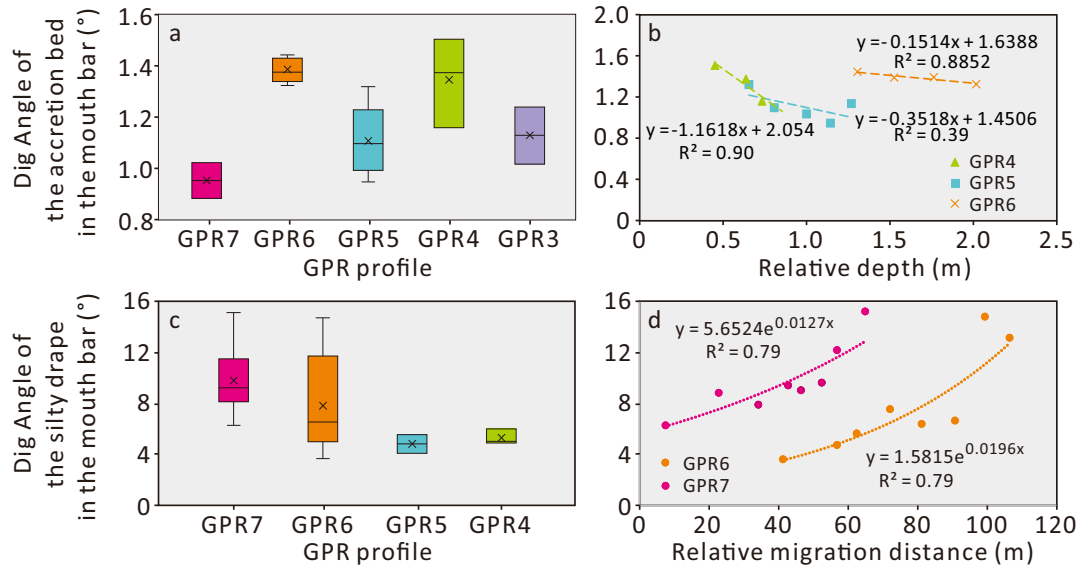

FIGURE 10: The dig angles of accretion beds of the mouth bar (a and b) and point bar (c and d) within GPR profiles of BSD5.

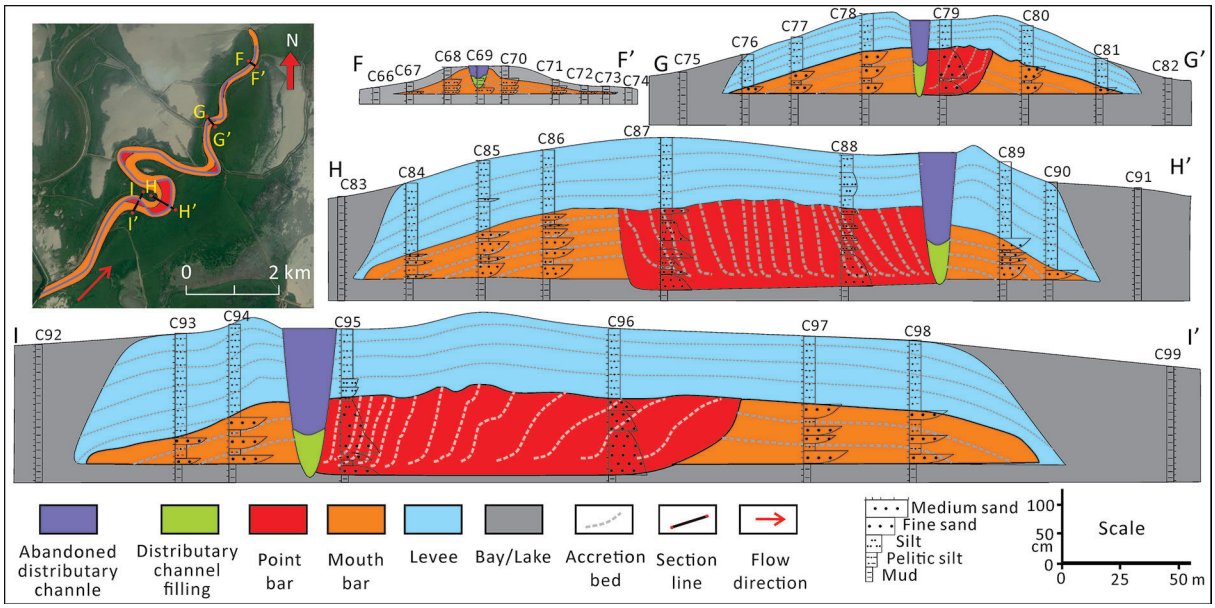

FIGURE 11: Architectural units within BSD5. Locations of the five cross-sections are indicated in the inset in the left corner as well as in Figure 3.

attention. Donaldson [15, 16] first proposed the architectural model of bar fingers within shallow-water deltas. They suggest: (1) the bar fingers consist of mouth bars, distributary channels, and levees, separated by interdistributary bays; (2) the distributary channel incises through the mouth bar, resulting in a wing-like mouth bar along the sides of the distributary channel; and (3) distributary channels are relatively straight. Xu et al. [24] argued that the bar fingers within the shallow-water delta are sinuous (sinuous index SI >1.1), which could be divided into high-R_{SI} and low-R_{SI} types. Low-R_{SI} bar finger develops a low sinuous distributary channel (sinuosity index <1.2) and thin levees, without the point bar, and the distributary channel incises the concave margin of the bar finger. High-R_{SI} bar finger develops a high sinuous distributary channel (sinuosity index ≥1.2) and thick levees, with point bars, and a distributary channel that incises the convex margin of the bar finger. On this basis, we find that the low-R_{SI} bar finger has a high elevation where the mouth bar domain is developed, and the elevation becomes low at the location of the mouth bar margin (Figures 8 and 12). In contrast, the high-R_{SI} bar finger has a high elevation where the mouth bar domain and point bar are developed, and the topography also becomes low at the location of the mouth bar margin (Figure 11). The levee is slightly wider than the mouth bar. In addition, the point bar is thick on

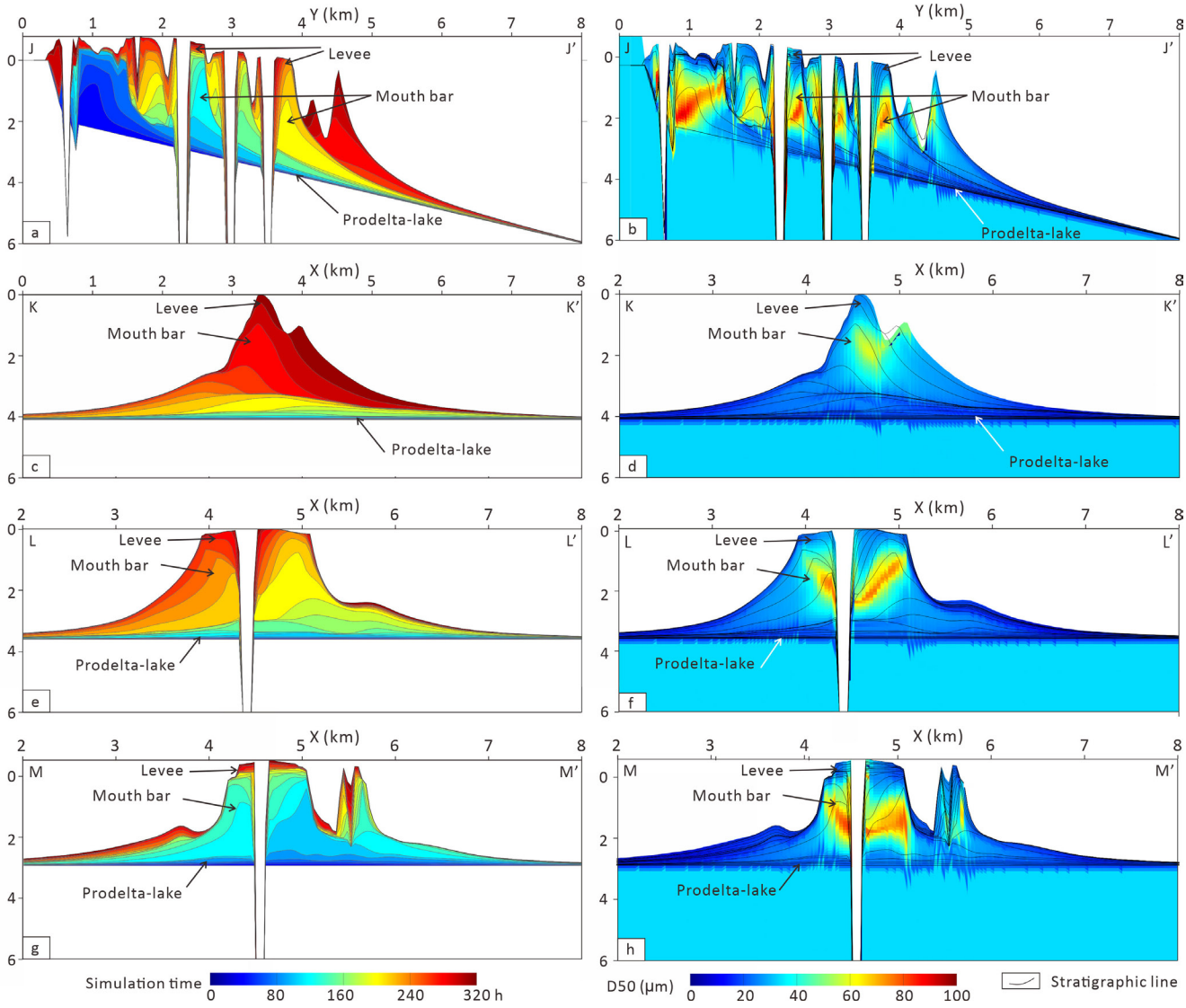

FIGURE 12: One longitudinal section and three cross sections of the stratigraphic evolution and grain size distribution in the simulated bar finger. The locations of the four sections are shown in Figure 5.

the distributary channel side and thin on the mouth bar side.

At present, nine-level architectural units in bar fingers are poorly documented. Based on field and simulated data, we established the architectural patterns of nine-level architectural units within low-R_{SI} and high-R_{SI} bar fingers.

5.1.1 Similar Architectural Patterns of Nine-Level Architectural Units Between Low-R_{SI} and High-R_{SI} Bar Fingers. The mouth bars develop multiple convex-up silty accretion beds. The accretion beds top lap the side of the distributary channel or point bar and down lap the bottom of the mouth bar. They have low dip angles (maybe <2°), and the upper accretion bed has a higher dip angle than the lower accretion bed. Additionally, the dip angle of the accretion bed increases slightly basinward. The coarsening-upward accretion sand bodies are interbedded by silty accretion beds. The levee developed multiple muddy horizontal accretion beds that separate the accretion silts.

5.1.2 Different Architectural Patterns of Nine-Level Architectural Units Between Low-R_{SI} and High-R_{SI} Bar Fingers. Low-R_{SI} and high-R_{SI} bar fingers exhibit differences in the architectural patterns of their nine-level architectural units in the following aspects:

(1) Accretion beds in the mouth bar. The accretion bed of the high-R_{SI} bar finger has a higher dip angle than that of the low-R_{SI} bar finger (0.8°–1.6° in BSD5 vs. 0.17°–0.7°in BSD6). The lower accretion bed within the high-R_{SI} bar finger has a dip angle of less than 1°, which is similar to the dip angle of the accretion bed in the low-R_{SI} bar finger. For the low-R_{SI} bar finger, the dip angle is higher at the outer bank of the

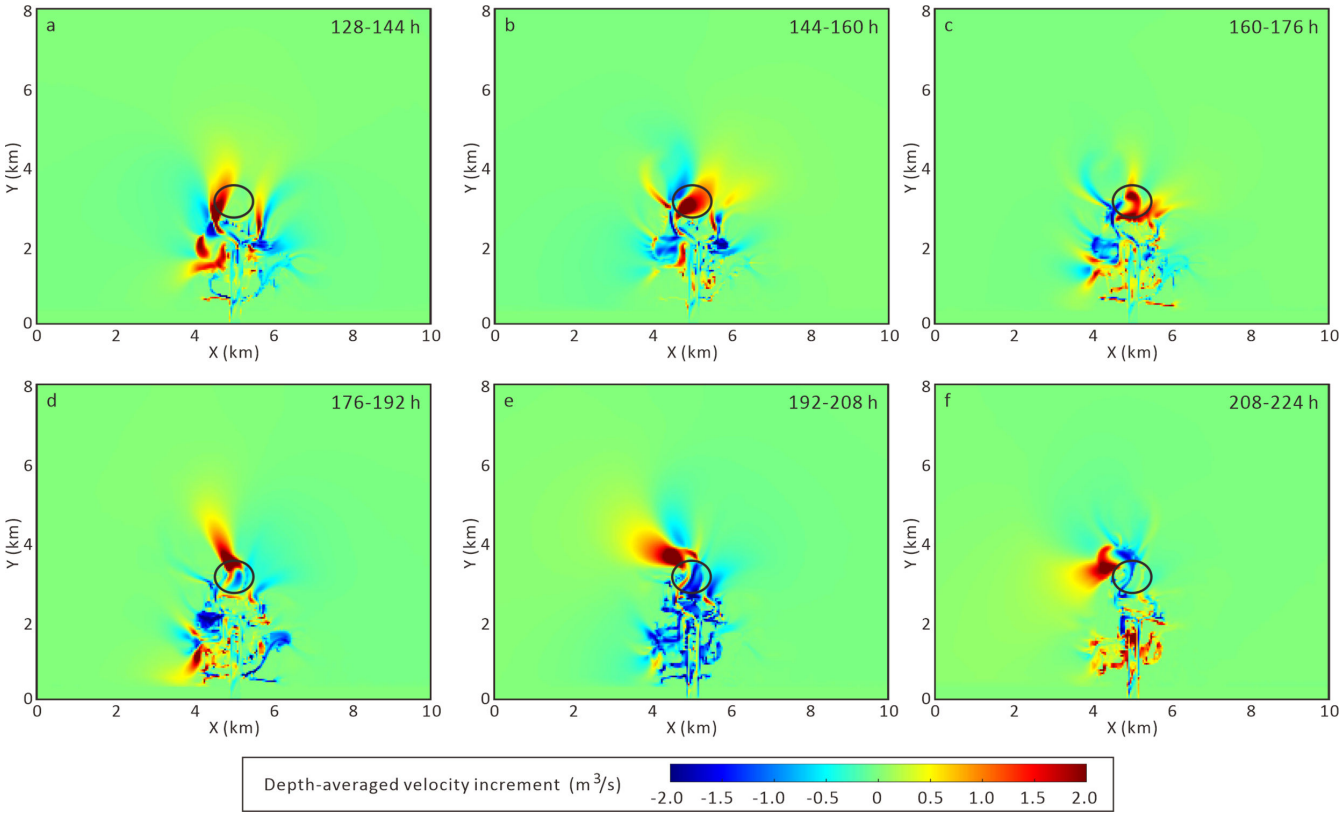

Figure 13: Map views of the depth-averaged velocity of water flow at selected simulated hours. The black circle illustrates the same location on different maps.

distributary channel, compared with the inner bank. In contrast, the dip angle is similar in both the banks of the distributary channels of high-R_{SI} bar fingers.

(2) Silty drapes (accretion beds) in the point bar. The point bar is unique to the high-R_{SI} bar finger, which develops multiple inclined silty drapes. The silty drapes top lap the top of the point bar. The dip angle of the silty drapes is high (4°–15° in BSD5), which decreases downstream and exponentially increases with lateral migration distance. The fining-upward accretion sand bodies are interbedded by silty drapes. The lateral spacing between adjacent silty drapes is small at the distributary channel side and large at the mouth bar side.

(3) Accretion beds in the levee. The thick levee in the high-R_{SI} bar finger develops many more accretion beds than the thin levee in the low-R_{SI} bar finger.

5.2 Formative Mechanism of Bar Finger Architecture Within Shallow-Water Delta. Previous research suggests that the formation of digitate deltas with bar fingers is dependent on high-cohesive and fine-grained sediments, which build cohesive levees and stable distributary channels [9, 10, 20]. The stable channel carries sediments, and the mouth bar is deposited at the outlet [41]. In the shallow-water environment, the rapidly deposited mouth bar can divert the outflow and redirect the distributary channel and resulting sinuous bar finger [24]. The central outflow has a higher velocity than the marginal outflow (Figure 13), so the central mouth bar becomes thick and coarse, compared with the marginal mouth bar. As a result, the mouth bar and its accretion beds form convex-up shapes (Figure 12). With the extension of the distributary channel, the velocity and spreading width of outflow become large (Figure 13(a)–13(c)), and thus, the younger (upper) accretion sand bodies in the mouth bar are wider and coarser than the older (lower) accretion sand bodies (Figure 12(g) and 12(h)). In addition, the upper accretion sand bodies overlay the lower convex-up accretion sand bodies, resulting in a high-dip angle in the upper accretion beds (Figure 12). The muddy/silty accretion beds of the mouth bar are not developed in the simulated bar finger due to a steady lake level (Figure 12). In nature, seasonal lake level fluctuation induces the deposition of the muddy/silty accretion bed [24, 42].

Initially, sinuous distributary channels could form as a result of lateral migration and change to high-sinuosity distributary channels, leading to the deposition of point bars in the inner banks of the distributary channels [24], similar to meandering river channels [43, 44]. The inclined silty drapes and concave scroll bars are all products of lateral channel migration [45–47]. However, the high-cohesive levee within the bar finger reduces the lateral migration distance of the distributary channel during flooding. In addition, the backwater effect near the river mouth could

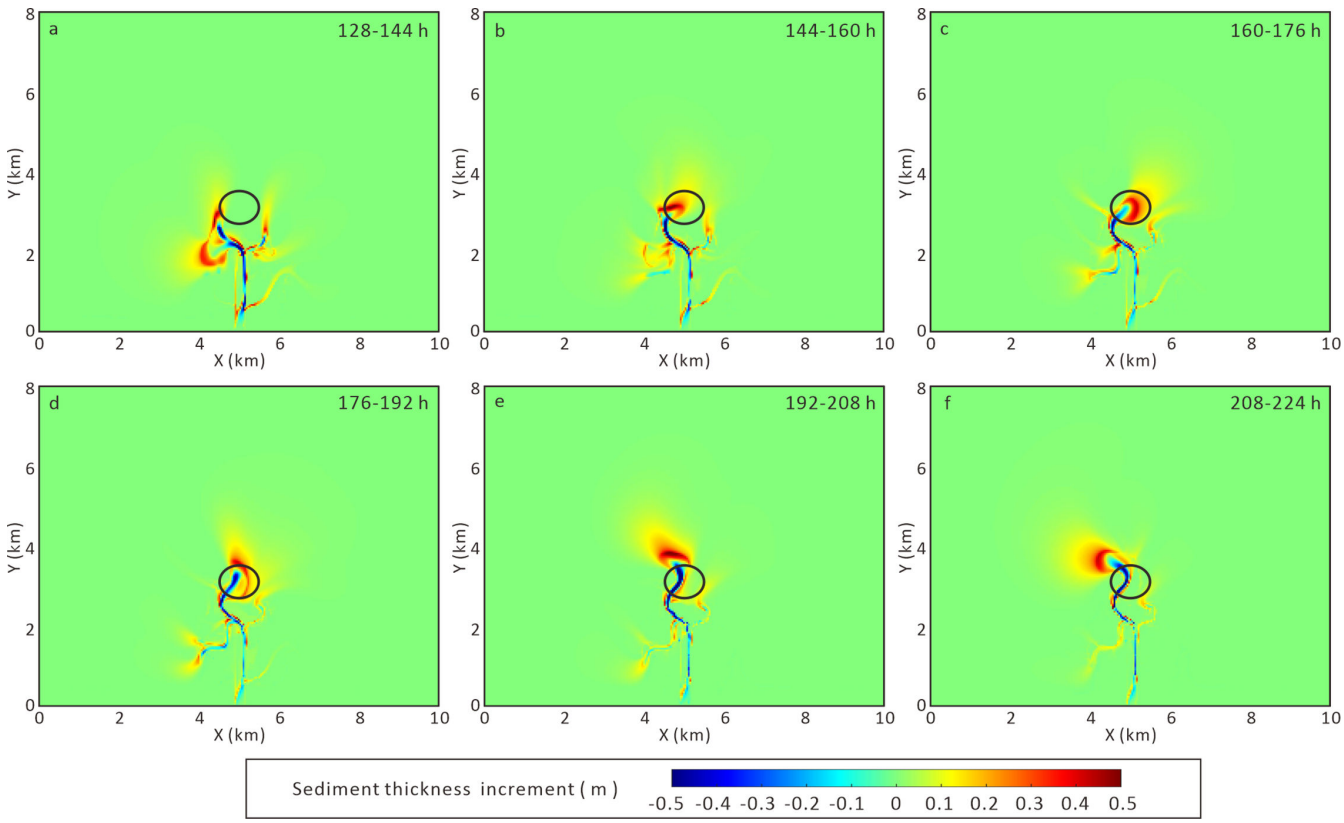

FIGURE 14: Map views of sediment thickness at select simulated hours. The black circle illustrates the same location on different maps. Negative sediment thickness indicates distributary channel incision, and positive sediment thickness indicates mouth bar and levee deposition.

weaken the centrifugal force of the distributary channel [48, 49] and reduce the lateral migration distance of the distributary channel during flooding. The dip angle of the silty drape exponentially increases with the lateral migration distance (Figure 10(d)). As a result, the silty drapes in the point bar within the bar finger have much larger dip angles (e.g., 4°–15° in BSD5), compared with that in the point bar within the upstream river (e.g., 3° in Laozhoutou point bar, Figure 4). The levee thins downstream (Figures 8 and 11), leading to a decrease in the dip angle of the silty drapes (Figure 10(c)).

5.3 Insights for the Prediction of Digitate Shallow-Water Delta Reservoirs. Digitate shallow-water delta reservoirs with bar fingers are commonly seen in petroliferous cratonic basins (e.g., Ordos Basin [50]; Bohai Bay Basin [23, 51]). The internal architectural pattern of bar fingers provides insights into the prediction and development of digitate shallow-water delta reservoirs. Here, we take two typical reservoirs as examples.

5.3.1 Example One: Chang 8 Subsection, Yanchang Formation, Triassic, Maling Area, Ordos Basin, China. The Maling Area is located in south Huanxian County, Shaanxi Province, China. Tectonically, it is located in the Tianhuan depression, western Ordos Basin [52] (Figure 15(a)). The Triassic Yanchang Formation is a significant oil-bearing interval, which is divided into ten subsections from top to bottom (Chang 1 to Chang 10) [53]. Chang 8–1 interval in the Chang-8 subsection contains digitate shallow-water deltas, which are low-porosity and extra-low-permeability reservoirs (average porosity is 6%–10%, and average permeability is 0.06–0.5 mD) [54].

Previous research suggests that the distributary channel (including point bar deposits) is the dominant depositional environment of the sandy deposits within the digitate shallow-water deltas of the Chang 8–1 interval [54, 55]. However, other researchers interpret the Chang 8–1 interval to represent bar fingers with both distributary channels and mouth bars [56, 57]. Based on previously published core and well-log data, we suggested that the Chang 8–1 interval represents high-R_{SI} bar fingers (Figure 15(b)–15(d)). Coarsening-upward mouth bar deposits are common (Figure 15(b) and 15(c)) and distributed at the sides of distributary channel deposits (Figure 15(d)). The levees are deposited on top of the distributary channel (Figure 15(d)). Distributary channels have high sinuosities (sinuosity index >1.2), and point bars are dominated by sandy distributary channel deposits (Figure 15(b) and 15(d)). The mouth bar contains 2–3 convex-up accretion beds with dig angles of 0.3°–1.5° (Figure 15(d)). The point bar develops 5–10 inclined silty drapes with dig angles of 5°–10° (Figure 15(d)). Our new interpretation will guide the analysis of the injection-production connection and the distribution of the remaining oil in the Chang 8–1 interval.

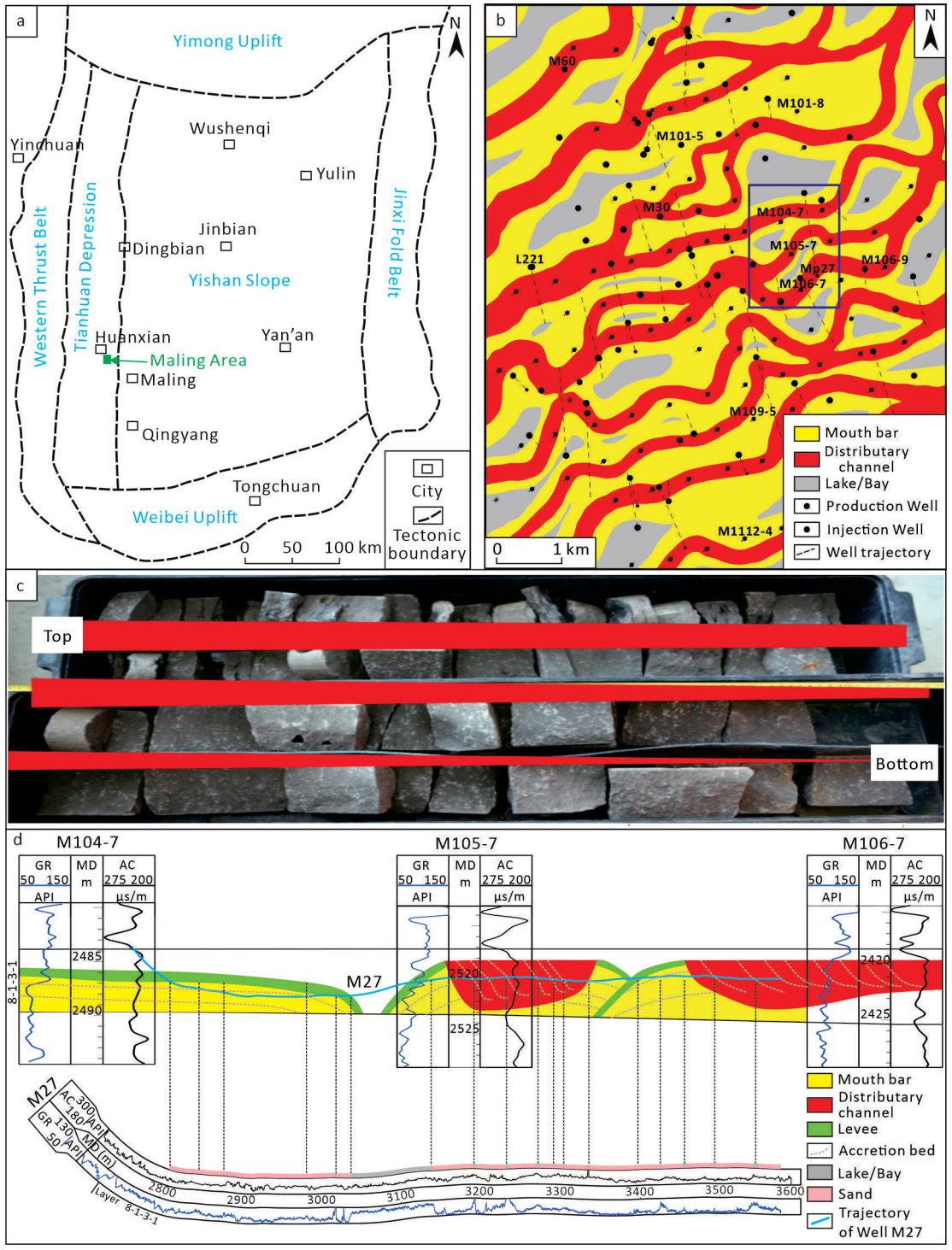

FIGURE 15: Digitate shallow-water delta reservoir with bar fingers in the Chang 8–1 interval, Triassic, Maling Area, Ordos Basin, China. (a) Map of the tectonic setting of the Ordos Basin and location of the Maling Area. (b) Distribution of eight-level architectural units in Layer 8-1-3-1. (c) Core photograph of potential coarsening-upward mouth bar deposits (Well M30, 2660.34–2662.76 m). (d) Well logs through Layer 8-1-3-1 at their architectural interpretation.

5.3.2 Example Two: Lower Minghuazhen Formation, Neogene, BZ Oilfield, Bohai Bay Basin, China. The BZ Oilfield is located in the marginal Huanghekou Sag of Bohai Bay, China (Figure 16(a)) [58, 59]. The target is the Lower Member of the Neogene Minghuazhen Formation, which is divided into I–VI Oil Groups. In the IV and V Oil Groups, digitate shallow-water deltas with bar fingers are the dominant petroliferous sand bodies [23, 60] (e.g., bar fingers in Layer V3.2 and IV8.2, illustrated in Figure 16(b) and 16(c)), which have a high porosity (average

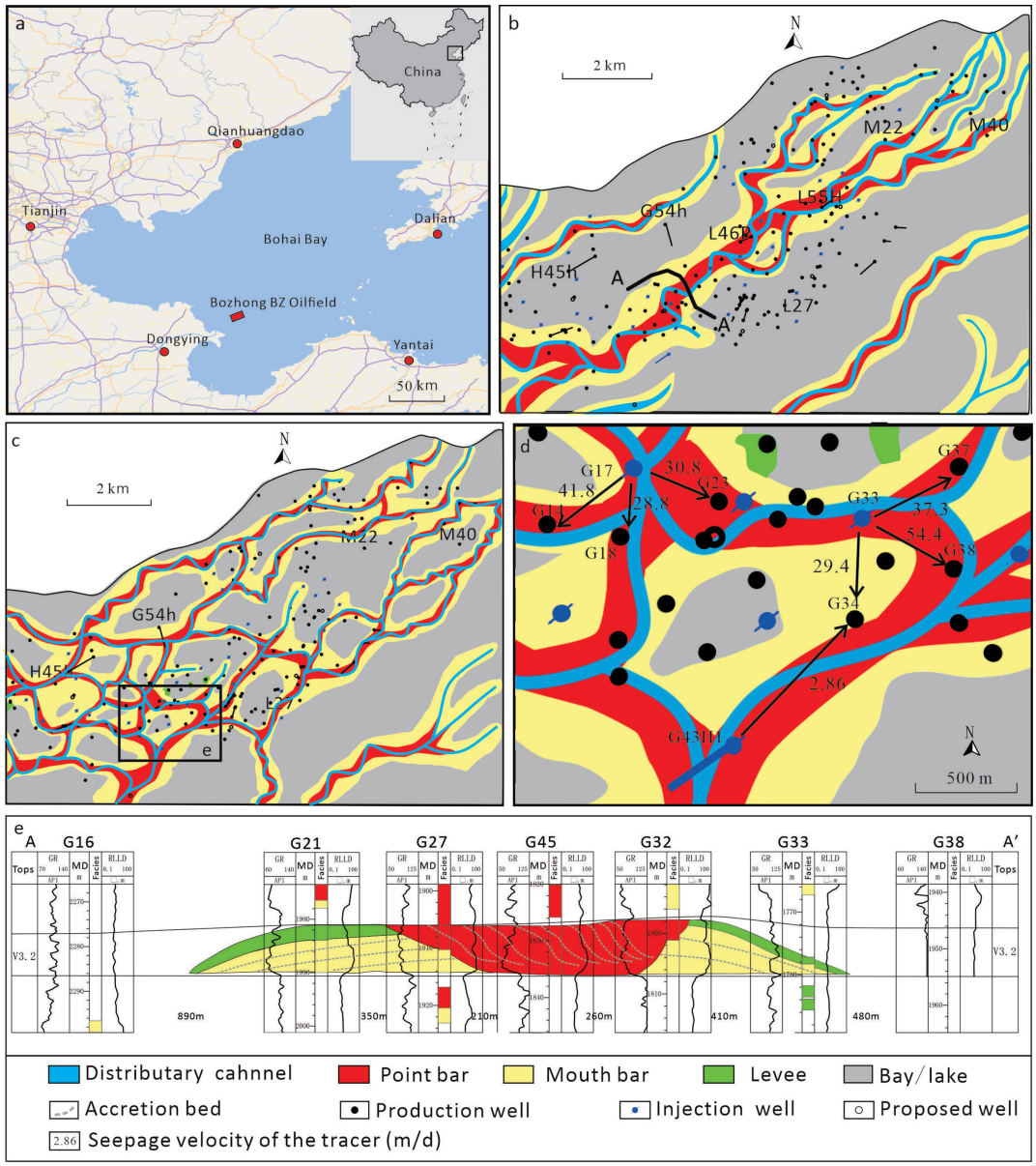

FIGURE 16: Digitate shallow-water delta reservoir with bar fingers in the Neogene Lower Minghuazhen Formation, BZ Oilfield, Bohai Bay Basin, China. (a) Map showing the BZ Oilfield. (b) Distribution of eight-level architectural units in Layer V3.2. (c) Architectural sections of Layer V3.2 in an area of dense well coverage. (d) The tracer test result of Layer IV8.2. (e) Well logs illustrating the distribution of eight-level architectural units in the Layer IV8.2.

value of 33%) and high permeability (average value of 2000 mD). However, it contains high-density and high-viscosity oil, so the reservoir recovery is only ~13.5%. An accurate prediction of the internal architecture within the bar fingers is critical to enhancing reservoir recovery.

Sandy distributary channel deposits within the bar fingers are mostly point bars, which are 1/3–1/5 times wider than the bar fingers themselves. Therefore, these bar fingers are of the high-sinuous type, and distributary channels incise their outer banks. Abandoned distributary channels with high sinuosities (>1.20) are observed within bar fingers (Figure 16(b) and 16(c)). The point bars are developed along the inner banks of the distributary channels. In addition, based on the architectural pattern, we observed accretion beds in mouth bars and point bars (Figure 16(e)). An average of three accretion beds are developed within the mouth bars, which have dip angles of ~0.5°. About ten silty drapes are developed within the point bars, which have dip angles of 5°–10°.

The architectural characteristics of the bar finger induce different water-flooding patterns in the sand body. The bottom of the point bar suffered severe water-flooding and the remaining oil accumulated in the middle-upper point bar [23] because inclined silty drapes reduce the sand body connectivity of the middle-upper point bars (Figure 16(e)). In contrast, the remaining oil only accumulated in the

upper mouth bar [23] because accretion beds have less of an influence on the sand body connectivity of the mouth bars and reduce the effects of gravity (Figure 16(e)).

The architectural characteristics of the bar fingers also affect the production rate of production wells. Based on tracer testing results in Layer IV8.2 (Figure 16(d)), we find the following four situations. Situation 1: If injection and production wells are located in the same point bar, the seepage velocity of the tracer is highest in the bottom of the point bar due to high connectivity and permeability (e.g., 41.8 m/d of seepage velocity between Well G17 and G14; 54.4 m/d of seepage velocity between Well G33 and G38). Situation 2: If injection and production wells are located in different point bars, the fine-grained abandoned distributary channel reduces the sand body connectivity so that the seepage velocity of the tracer is lower than that in Situation 1 (e.g., 37.3 m/d of seepage velocity between Well G33 and G37; 28.8 m/d of seepage velocity between Well G17 and G18). Situation 3: If injection and production wells are located in adjacent point and mouth bars, the seepage velocity of the tracer is lower than that of Situation 2 due to different architectural patterns of accretion beds between point bars and mouth bars (e.g., 29.4 m/d of seepage velocity between Well G33 and G34). Situation 4: If injection and production wells are located in the point bar and mouth bar individually and are separated by an abandoned distributary channel, the seepage velocity of the tracer is lowest (e.g., 2.86 m/d of seepage velocity between Well G43H1 and G34).

6. Conclusions

This paper examines the internal architecture of the sinuous bar fingers of a digitate shallow-water delta, which consists of a distributary channel, mouth bars, and levees, as well as point bars in the high-R_{SI} (sinuosity index ≥1.20) bar finger.

Mouth bars develop several convex-up accretion beds, which top lap the side of the distributary channels or point bars and down lap the bottom of the mouth bars. The central outflow has a higher velocity than the marginal outflow, so the central mouth bar is thicker and coarser than the marginal mouth bar, leading to the formation of the convex-up accretion beds, with low dip angles (<2°). With the extension of the distributary channel, the velocity and spreading width of the outflow become large, leading the upper accretion bed to have a higher dip angle than the lower accretion bed.

The point bars in the high-R_{SI} bar fingers develop multiple inclined accretion beds (i.e., silty drapes), which top lap the top of the point bar. The dip angle of the accretion bed (>10°) is much higher than that in the supplying river because the cohesive levee and backwater effect reduces the lateral migration distance of the distributary channel. The dip angle decreases downstream and exponentially increases with the lateral migration distance. The lateral spacing between the adjacent lateral accretion beds is smaller near the distributary channel and large near the mouth bar. The levee thins downstream (figures 8 and 11), leading to a decrease in the dig angle of silty drapes.

The levee develops multiple horizontal muddy accretion beds. The thick levee in the high-R_{SI} bar finger develops many more accretion beds than the thin levee in the low-R_{SI} bar finger.

The results of this paper provide insights into the prediction and development of cratonic digitate shallow-water delta reservoirs, such as in the Chang 8 subsection, Yanchang Formation, Triassic, Maling Area, Ordos Basin, China and in the Lower Minghuazhen Formation, Neogene, BZ Oilfield, Bohai Bay Basin, China.

Data Availability

The simulation data (the model domain and output mat data) in this paper are uploaded in the Mendeley data and could be found from http://dx.doi.org/10.17632/hxmcbgk6g7.1.

Conflicts of Interest

We confirm that we have no known competing financial interests or personal relationships that could have appeared to influence the work reported in this paper.

Acknowledgments

The work presented in the paper was financially supported by the National Natural Science Foundations of China (No. 42202178 and 42130813), and the China Postdoctoral Science Foundation (No.2022M720540). We thank A. P. Burpee for help with the Delft3D simulations. We are very grateful to the Guest Editors Simms Alexander R. and Xiangyang Xie, and other anonymous reviewers for constructive reviews that significantly improved the manuscript.

References

[1] R. L. Caldwell, D. A. Edmonds, S. Baumgardner, C. Paola, S. Roy, and J. H. Nienhuis, "A global Delta Dataset and the environmental variables that predict Delta formation on marine coastlines, " *Earth Surface Dynamics*, vol. 7, no. 3, pp. 773–787, 2019.

[2] B. Willis and T. Sun, "Relating Depositional processes of river-dominated deltas to reservoir behavior using computational Stratigraphy," *The Journal of Sedimentary Research*, vol. 89, no. 3, pp. 1250–1276, 2019.

[3] D. A. Edmonds, R. L. Caldwell, E. S. Brondizio, and S. M. O. Siani, "Coastal flooding will disproportionately impact people on river deltas," *Nature Communications*, vol. 11, no. 1, 2020.

[4] J. H. Nienhuis, A. D. Ashton, D. A. Edmonds, et al., "Global-scale human impact on Delta morphology has led to net land area gain," *Nature*, vol. 577, no. 7791, pp. 514–518, 2020.

[5] H. A. Bernard, "A resume of river Delta types: Abstract," *AAPG Bulletin*, vol. 49, 1965.

[6] W. L. Fisher, L. F. Brown, A. J. Scott, et al, *Delta Systems in the Exploration for Oil and Gas. Bureau of Economic Geology*, University of Texas, Austin, TX, 1969.

[7] A. J. Dumars, *Distributary Mouth Bar Formation and Channel Bifurcation in the Wax Lake Delta, Atchafalaya Bay, Louisiana*, Louisiana State University, Baton Rouge, 2002.

[8] C. Olariu and J. P. Bhattacharya, "Terminal Distributary channels and Delta front architecture of river–dominated Delta systems," *Journal of Sedimentary Research*, vol. 76, no. 2, pp. 212–233, 2006.

[9] A. P. Burpee, R. L. Slingerland, D. A. Edmonds, et al., "Grain–size controls on the morphology and internal geometry of river–dominated deltas," *Journal of Sedimentary Research*, vol. 85, no. 6, pp. 699–714, 2015.

[10] R. L. Caldwell and D. A. Edmonds, "The effects of sediment properties on Deltaic processes and Morphologies: A numerical modeling study," *Journal of Geophysical Research*, vol. 119, no. 5, pp. 961–982, 2014.

[11] H. N. Fisk, C. R. Kolb, E. McFarlan, and L. J. Wilbert, "Sedimentary framework of the modern Mississippi Delta," *Journal of Sedimentary Research*, vol. 24, no. 2, pp. 76–99, 1954.

[12] C. C. Bates, "Rational theory of Delta formation," *AAPG Bull*, vol. 37, pp. 2119–2162, 1953.

[13] H. N. Fisk, "Sand Facies of recent Mississippi Delta deposit," in *4th World Petroleum Congress*, pp. 377–398, Rome, Italy, 1955.

[14] F. H. N, "Bar-finger sands of Mississippi Delta," in *Geometry of Sandstone Bodies* J.A. Peterson, and J.C. Osmond, Eds., pp. 29–52, Am Assoc. Petrol. Geologists, Tulsa, Okla, 1961.

[15] A. C. Donaldson, "Deltaic sands and Sandstones," in *20th Annual Conference*, pp. 31–62, 1966.

[16] A. C. Donaldson, "Pennsylvanian sedimentation of central Appalachians," Special Paper of the Geological Society of America, vol. 148, pp. 47–48, 1974.

[17] W. E. Galloway, *Process Framework for Describing the Morphologic and Stratigraphic Evolution of Deltaic Depositional Systems, Deltas: Models for Exploration*, Houston Geological Society, Houston, Texas, 1975.

[18] W. Kim, A. Dai, T. Muto, and G. Parker, "Delta Progradation driven by an advancing sediment source: Coupled theory and experiment describing the evolution of elongated deltas," *Water Resources Research*, vol. 45, no. 6, 2009.

[19] J. C. Rowland, W. E. Dietrich, G. Day, and G. Parker, "Formation and maintenance of Single-Thread tie channels entering Floodplain lakes: Observations from three diverse river systems," *Journal of Geophysical Research*, vol. 114, no. F2, 2009.

[20] D. A. Edmonds and R. L. Slingerland, "Stability of Delta Distributary networks and their Bifurcations," *Water Resources Research*, vol. 44, no. 9, 2008.

[21] D. A. Edmonds, J. B. Shaw, and D. Mohrig, "Topset-dominated deltas: A new model for river Delta Stratigraphy," *Geology*, vol. 39, no. 12, pp. 1175–1178, 2011.

[22] S. Wu, Z. Xu, and Z. Liu, "Depositional architecture of Fluvial-dominated shoal water Delta," *Journal of Palaeogeography*, vol. 21, no. 2, pp. 202–215, 2019.

[23] Z. Xu, S. Wu, Z. Liu, et al., "Reservoir architecture of the finger bar within shoal water Delta front: Insights from the lower member of Minghuazhen formation, Neogene, Bohai Bz25 oilfield, Bohai Bay Basin, East China," *Petroleum Exploration and Development*, vol. 46, no. 2, pp. 335–346, 2019.

[24] Z. Xu, P. Plink-Björklund, S. Wu, et al, "Sinuous bar fingers of Digitate shallow-water deltas: Insights into their formative processes and deposits from integrating morphological and Sedimentological studies with mathematical Modelling," *Sedimentology*, vol. 69, no. 2, pp. 724–749, 2022.

[25] D. Yue, W. Li, W. Wang, et al., "Analyzing the architecture of point bar of meandering Fluvial river using ground penetration radar: A case study from Hulun Lake depression, China," *Interpretation*, vol. 7, no. 2, pp. T437–T454, 2019.

[26] M. Słowik, "Changes of river bed pattern and traces of Anthropogenic intervention: The example of using GPR method (the Obra river, Western Poland)," *Applied Geography*, vol. 31, no. 2, pp. 784–799, 2011.

[27] B. Liu, C. Tan, X. Yu, X. Shan, and S. Li, "Evolution model of a modern Delta Fed by a seasonal river in Daihai lake, North China: Determined from ground-penetrating radar and trenches," *Frontiers of Earth Science*, vol. 13, no. 2, pp. 262–276, 2019.

[28] C. Tan, P. Plink-BjÖrklund, and S. Hubbard, "Morphodynamics of supercritical flow in a linked river and Delta system, Daihai lake, Northern China," *Sedimentology*, vol. 68, no. 4, pp. 1606–1639, 2021.

[29] D. Shankman, B. D. Keim, and J. Song, "Flood frequency in China's Poyang Lake region: Tends and Teleconnections," *International Journal of Climatology*, vol. 26, no. 9, pp. 1255–1266, 2006. http://doi.wiley.com/10.1002/joc.v26:9.

[30] Z. Yin and J. Zhang, "The Hydrological features of Poyang Lake," *Oceanologia et Limnologia Sinica*, vol. 18, pp. 22–27, 1987.

[31] Y. Fang, "Ganjiang river," *Yangtze River*, vol. 7, pp. 22–25, 1956.

[32] Q. Tan, "The historical process of the evolution of Poyang Lake," *Fudan Journal of the Humanities and Social Sciences*, vol. 2, pp. 42–51, 1982.

[33] G. R. Lesser, J. A. Roelvink, J. A. T. M. van Kester, and G. S. Stelling, "Development and validation of a three-dimensional morphological model," *Coastal Engineering*, vol. 51, nos. 8–9, pp. 883–915, 2004.

[34] R. Marciano, Z. Wang, and A. Hibma, "Modeling of channel patterns in short tidal basins," *Journal of Geophysical Research*, vol. 110, no. F1, 2005.

[35] L. C. van Rijn, *Principles of Sediment Transport in Rivers, Estuaries, and Coastal Seas*, Aqua publications, Amsterdam, 1993.

[36] W. Feng, S. Wu, K. Zhang, et al, "Depositional process and sedimentary model of meandering–river shallow Delta: Insights from numerical simulation and modern deposition," *Acta Geologica Sinica*, vol. 91, pp. 2047–2064, 2017.

[37] Z. Xu, S. Wu, D. Yue, et al., "Effects of upstream conditions on Digitate shallow-water Delta morphology," *Marine and Petroleum Geology*, vol. 134, December, p. 105333, 2021.

[38] S. Wu, Y. Ji, D. Yue, et al, "Discussion on Hierarchical scheme of architectural units in Clastic deposits," *Geological Journal of China Universities*, vol. 19, no. 1, pp. 12–22, 2013.

[39] I. Ll. van Heerden, J. T. Wells, and H. H. Roberts, "River-dominated suspended sediment deposition in a new

Mississippi Delta," *Canadian Journal of Fisheries and Aquatic Sciences*, vol. 40, no. S1, pp. s60–s71, 1983.

[40] D. R. Cahoon, D. A. White, and J. C. Lynch, "Sediment Infilling and Wetland formation Dynamics in an active crevasse Splay of the Mississippi River Delta," *Geomorphology*, vol. 131, nos. 3–4, pp. 57–68, 2011.

[41] D. A. Edmonds and R. L. Slingerland, "Mechanics of river mouth bar formation: Implications for the Morphodynamics of Delta Distributary networks," *Journal of Geophysical Research*, vol. 112, no. F2, 2007.

[42] Y. Zhang, L. Qiu, B. Yang, J. Li, and Y. Wang, "Effects of water level fluctuation on sedimentary characteristics and reservoir architecture of a lake, river dominated Delta," *Journal of Central South University*, vol. 23, no. 11, pp. 2958–2971, 2016.

[43] H. Johannesson and G. Parker, "Linear theory of river Meanders," in *River meandering*, S. Ikeda, and G. Parker, Eds., 12:pp. 181–213, AGU, Water Resources Monograph, 1989.

[44] Y. Peng, C. A. Hagstrom, S. C. Horner, et al., "Low-accommodation foreland Basin response to long-term transgression: A record of change from Continental-Fluvial and marginal-marine to open-marine sequences over 60,000 Km2 in the Western Canada foreland Basin," *Marine and Petroleum Geology*, vol. 139, May, p. 105583, 2022.

[45] F. Schuurman, Y. Shimizu, T. Iwasaki, and M. G. Kleinhans, "Dynamic meandering in response to upstream perturbations and Floodplain formation," *Geomorphology*, vol. 253, January, pp. 94–109, 2016.

[46] R. J. P. Strick, P. J. Ashworth, G. Awcock, and J. Lewin, "Morphology and spacing of river Meander scrolls," *Geomorphology*, vol. 310, June, pp. 57–68, 2018.

[47] Y. Wang, T. F. Baars, H. Sahoo, et al., "Sandstone body character and river Planform styles of the lower Eocene Willwood formation, Bighorn Basin, Wyoming, USA," *Sedimentology*, vol. 69, no. 7, pp. 2897–2924, 2022. https://onlinelibrary.wiley.com/toc/13653091/69/7.

[48] D. A. Edmonds, D. C. J. D. Hoyal, B. A. Sheets, and R. L. Slingerland, "Predicting Delta Avulsions: Implications for Coastal Wetland restoration," *Geology*, vol. 37, no. 8, pp. 759–762, 2009.

[49] D. C. J. D. Hoyal and B. A. Sheets, "Morphodynamic evolution of experimental cohesive deltas," *Journal of Geophysical Research*, vol. 114, no. F2, 2009.

[50] C. Hu, H. Qu, J. Miao, et al, "A study on sedimentary Microfacies and oil-bearing possibility in Chang 6 oil-bearing formation in the area of Nanniwan," *Journal of Northwest University (Natural Science Edition)*, vol. 38, no. 6, pp. 994–1000, 2008.

[51] J. Zhang, M. Wang, Y. Wang, et al, "Identification and sedimentary evolution of the shallow water Delta of bird-foot in Bozhong 28-2S oilfield group of Bohai Bay Basin," *Periodical of Ocean University of China*, vol. 47, no. 9, pp. 77–85, 2017.

[52] Y. Duan, Y. Yuan, and R. Qian, "Migration features of crude oil in Fluvial deposits of Maling oilfield in Ordos Basin, China," *Organic Geochemistry*, vol. 58, May, pp. 78–85, 2013.

[53] Y. Duan, "Geochemical characteristics of crude oil in Fluvial deposits from Maling oilfield of Ordos Basin, China," *Organic Geochemistry*, vol. 52, November, pp. 35–43, 2012.

[54] B. Ye, J. Ma, L. Shi, et al, "Control factors and distribution regularity of Chang 81 high quality reservoir in Maling area, Ordos Basin," *Journal of Xi'an University of Science and Technology*, vol. 39, no. 6, pp. 1016–1025, 2019.

[55] C. Ma, R. Wang, B. Luo, et al, "Characteristics of Chang 8 oil reservoir and distribution of oil reservoirs in Maling oilfield, Ordos Basin," *Natural Gas Geoscience*, vol. 23, no. 3, pp. 514–519, 2012.

[56] X. Si and J. Zhang, "Sedimentary Facies and hydrocarbon distribution law in Chang 8 reservoirs, Xifeng oilfield," *Journal of Southwest Petroleum University (Science & Technology Edition)*, vol. 30, no. 6, pp. 67–71, 2008.

[57] T. Wang, X. Deng, S. Wu, et al, "Differential distribution mechanism of tight Sandstone oil by the reservoir properties in scale of single layer: A case of the Chang 81 reservoirs in Yanchang formation, Huaqing area, Ordos Basin," *Journal of Northwest University (Natural Science Edition)*, vol. 49, no. 3, pp. 395–405, 2019.

[58] D. Jia, X. Yang, X. Wu, et al, "Study of restraining barrier and Interbeds in shallow water Delta Facies controlled by middle well-pattern density-taking Bozhong 25-1 Nan oilfield as example," *Petroleum Geology and Recovery Efficiency*, vol. 12, no. 2, pp. 19–22, 2005.

[59] H. Meng, D. Zhong, C. Li, et al, "Sedimentary Facies and evolution of the member 2 of Paleogene Shahejie formation of Bz25-1 oilfield in Bozhong depression, Bohai Bay Basin," *Journal of Paleogeography*, vol. 18, no. 2, pp. 161–172, 2016.

[60] Y. Hu, K. Huang, and Z. Xu, "Distribution character of remaining oil with finger bar of bird-foot shoal water Delta reservoir in BZ oilfield, Bohai Bay Basin," *Bulletin of Geological Science and Technology*, vol. 38, no. 2, pp. 189–198, 2019.